CrossMark

ORIGINAL PAPER

Dynamic Tensile Strength of Coal under Dry and Saturated Conditions

Yixin Zhao[1,2] · Shimin Liu[3] · Yaodong Jiang[1] · Kai Wang[2] · Yaqiong Huang[1]

Abstract The tensile failure characterization of dry and saturated coals under different impact loading conditions was experimentally investigated using a Split Hopkinson pressure bar. Indirect dynamic Brazilian disc tension tests for coals were carried out. The indirect tensile strengths for different bedding angles under different impact velocities, strain rates and loading rates are analyzed and discussed. A high-speed high-resolution digital camera was employed to capture and record the dynamic failure process of coal specimens. Based on the experimental results, it was found that the saturated specimens have stronger loading rate dependence than the dry specimens. The bedding angle has a smaller effect on the dynamic indirect tensile strength compared to the impact velocity. Both shear and tensile failures were observed in the tested coal specimens. Saturated coal specimens have higher indirect tensile strength than dry ones.

Keywords Split Hopkinson pressure bar · Coal · Tensile strength · Water saturated

✉ Yixin Zhao
zhaoyx@cumtb.edu.cn

1   State Key Laboratory of Coal Resources and Safe Mining, China University of Mining and Technology, Beijing 100083, China

2   College of Resources and Safety Engineering, China University of Mining and Technology, Beijing 100083, China

3   Department of Energy and Mineral Engineering, G3 Center and EMS Energy Institute, Pennsylvania State University, University Park, PA 16802, USA
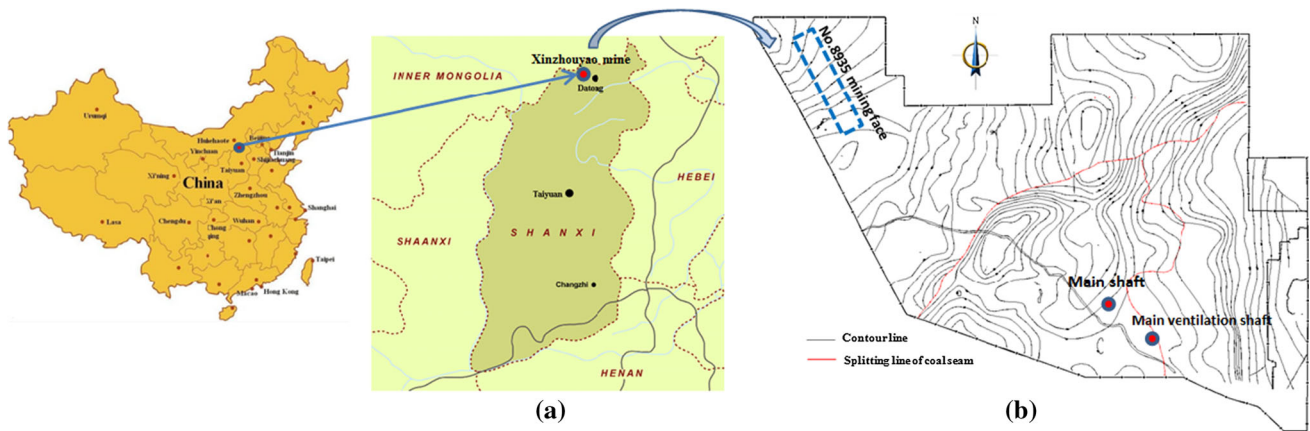
1 Introduction

The mechanical properties, e.g., the compressive and tensile strengths, elastic moduli, Poisson's ratio and fracture stiffness of rocks are strain/loading rate dependent, and are known as dynamic rock properties. Among these dynamic properties, the dynamic tensile strength is the subject of great interest, not only for the underground engineers (mining, geotechnical and tunneling engineers), but also for other branches of engineering, such as mineral processing, where the main objective is associated with energy consumption during mineral/rock crushing and milling.

From the mining engineering point of view, the interest with respect to the dynamic tensile strength of rock is very often associated with the fracture initiation, propagation and failure that can develop in the pillars, roof, floor and caving zone, and in the gob during continuous mining. The underground rock and/or rock mass encounters dynamic or cyclic loading induced by drilling and blasting, mechanized extraction, hydraulic support advance, periodical caving, tectonic movement, or combinations of these effects. Because of such dynamic loading, the ground control is challenging due to the lack of comprehensive dynamic rock properties. During the mine design, the dynamic rock mechanical properties should be considered and incorporated in the ground control and rock/coal burst control plans. To improve the mining safety conditions, dynamic rock properties need to be thoroughly investigated and incorporated in the mine design and ground control plans. The dynamic tensile strength is the focus of this study.

Most recently, a comprehensive review of the dynamic testing of rock material has been provided by Zhang and Zhao (2013a, b, c). Considerable research efforts have been devoted over the last 50 years to characterize the dynamic

🖄 Springer

Fig. 1 Location of the Xinzhouyao coal mine: **a** location of the Xinzhouyao mine in Shanxi Province; **b** boundary of Xinzhouyao coal mine with contour lines and sampling face
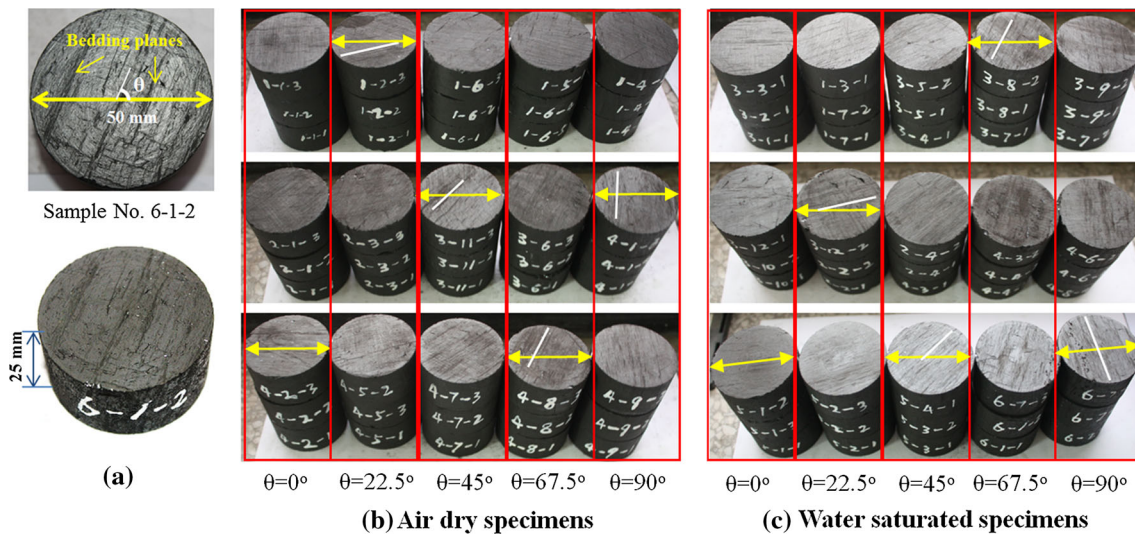

Fig. 2 BD specimens for the SHPB tests: **a** dimension of specimen and bedding angle (θ); **b** 45 air dry specimens with different bedding angles; **c** 45 water-saturated specimens with different bedding angles (color figure online)

tensile behavior of rocks, such as sandstone (Fuenkajorn and Kenkhunthod 2010; Gong and Zhao 2013; Huang et al. 2010; Ray et al. 1999), granite (Cho et al. 2003; Dai et al. 2010; Dutta and Kim 1993; Goldsmith et al. 1976; Khan and Irani 1987; Zhao et al. 1999), tuff (Asprone et al. 2009; Cho et al. 2003; Yan et al. 2012), marble (Howe et al. 1974; Wang et al. 2009; Q.B. Zhang and Zhao 2013a) and shale (Cai et al. 2007; Mclamore and Gray 1967; Xia et al. 2010) using both direct tension and indirect tension methods. However, to the best of our knowledge, the dynamic tensile behavior of coal has not been fully studied. Compared with other rocks, coal is known as a complex heterogeneous and anisotropic porous rock. The microstructure of coal usually contains complex networks of discontinuities or bedding planes (Scholtès et al. 2011) resulting in the fact that it is more challenging to characterize its dynamic behaviors and estimate its dynamic

properties. Also, the dynamic tensile strength of coals is expected to be affected by the moisture. A number of studies have attempted to analyze the impact of moisture on the strength of rocks. The majority of these studies focused on the influence of moisture on the uniaxial compressive strength (UCS) and found that the UCS of saturated coals is usually smaller than for dry ones (Burshtein 1969; Colback and Wiid 1965; Hawkins and Mcconnell 1992). Efforts have also been devoted to investigate the influence of water content on the rock mechanical properties, including tensile strength (Han 2003), triaxial strength (Han 2003; Li and Reddish 2004), point loading strength (Broch 1979) and the dynamic indirect tensile strength (Huang et al. 2010). For the dynamic tensile strength of rock, it was shown that the saturated specimen has stronger loading rate sensitivity than dry specimen, and the water softening factor decreases
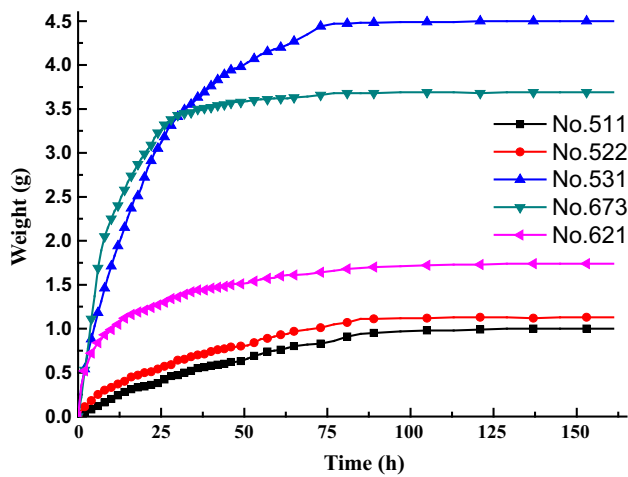
Fig. 3 Water imbibing process curves for five typical specimens

with the loading rate (Huang et al. 2010). For coals, however, the influence of water content on its dynamic tensile strength has not been studied. Furthermore, given the complex coal fracture geometry, no effort has been made to study the combined influence of beddings and moisture on tensile failure behavior under dynamic load.

In this study, the dynamic indirect tensile strength of coal using the Brazilian disc (BD) test was investigated under both dry and saturated conditions. The dynamic indirect tensile tests were conducted using a split Hopkinson pressure bar (SHPB) system at the China University of Mining and Technology, Beijing (CUMTB). The effects of impact velocity, nominal strain rate, loading rate and angle of bedding plane on the dynamic failure of coal were studied. A high-speed camera was employed to monitor the dynamic deformation and cracking evolution. Moreover, the post-failure coal fragments were analyzed to characterize the dynamic failure features for both dry and saturated coals.

2 Experimental Work

2.1 Specimen Procuration and Preparation

Fresh coal blocks were collected from No. 11 coal seam in the Xinzhouyao coal mine in Dadong City, Shanxi Province, China. The geographical location of the mine is shown in Fig. 1. The coal blocks were cut from the No. 8935 working face, and the face location is also shown in Fig. 1. The coal proximate analysis was carried out in our

(a) SHPB system
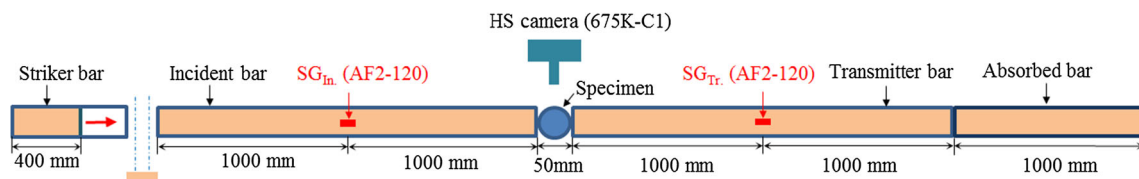
(b) Schematic of the setup of SHPB sysem

Fig. 4 The SHPB of the State Key Laboratory for Geomechanics and Deep Underground Engineering of CUMTB and the test setup of the dynamic indirect tensile strength test

Table 1 Final results of the dynamic indirect tensile test on 32 air dry coal specimens

Specimen ID	Bedding direction (°)	Impact velocity (m/s)	Strain rate (s^{-1})	Failure time (μs)	Dynamic indirect tensile strength (MPa)
421	0.0	2.701	55.827	130	4.272
211	0.0	3.213	54.855	130	4.942
112	0.0	3.328	58.947	139	4.998
113	0.0	3.487	73.735	129	5.113
212	0.0	3.565	74.326	161	5.263
122	22.5	2.378	54.758	133	4.001
232	22.5	2.518	56.103	177	4.206
233	22.5	2.565	56.194	172	4.301
452	22.5	2.972	54.327	170	4.587
121	22.5	3.298	63.848	156	5.100
453	22.5	3.803	72.446	120	5.441
161	45.0	2.624	49.389	165	4.583
162	45.0	3.146	58.824	141	5.011
472	45.0	3.226	58.118	119	5.193
471	45.0	3.768	68.421	116	5.709
3111	45.0	3.882	75.594	123	5.905
3113	45.0	3.884	95.895	138	5.917
481	67.5	2.125	39.395	124	3.730
482	67.5	2.689	52.053	127	4.380
151	67.5	3.286	65.897	135	5.375
363	67.5	3.332	60.992	108	5.306
362	67.5	3.448	72.750	130	5.405
165	67.5	3.689	73.390	131	5.409
164	67.5	3.703	73.565	189	5.507
361	67.5	4.008	79.009	162	5.733
491	90.0	2.105	40.747	121	3.893
492	90.0	2.113	37.776	160	3.897
412	90.0	2.336	41.466	181	3.923
411	90.0	2.779	50.390	157	4.862
413	90.0	2.970	54.737	206	4.862
493	90.0	3.018	52.237	194	5.051
143	90.0	3.843	73.487	147	5.860

laboratory (ASTM D5142 2009). The coal specimens are bituminous coals, with vitrinite reflectance (R_o) of 0.76–0.85 %, moisture of 4.0 %, ash content of 2.3 %, volatile matter of 25.0 % and fixed carbon content of 68.7 %. The porosity of coal is 28 % based on mercury intrusion porosimetry. The bulk densities of dry and saturated coals were ∼1.32 and ∼1.34 g/cm³, respectively.

A number of cylindrical cores with a diameter of 50 mm were drilled parallel to beddings from a single big coal block. Then, the cores were trimmed to circular discs with thickness of ∼25 mm. And the two end planes of each specimen were ground to ensure that both planes were parallel with accuracy of ±0.05 mm and both planes were perpendicular to the longitudinal axis with accuracy of

±0.25°. This dimension of the coal discs used for the subsequent indirect tensile strength tests is in accordance with the ISRM recommended size for Brazilian rock tests (ISRM 1978; Zhou et al. 2012). A typical top and side view of the prepared specimen is illustrated in Fig. 2a. The bedding angle, θ, was defined as the angle between the impact direction (the yellow double-ended arrow direction) and bedding planes as shown in Fig. 2a.

A total of 90 disc specimens were finally prepared as shown in Fig. 2. Half of the specimens were kept air dry and the rest were immersed in a water bath for 161 h to achieve saturated conditions. Both air dry and water-saturated specimens were separated into five groups based on the different bedding angles. Figure 2b shows 45 air dry specimens with bedding angle from 0° to 90° with an

interval of 22.5°. Figure 2c presents the 45 water-saturated specimens with the bedding geometries analogous to the air dry specimens.

For the saturated coal specimens, to ensure full saturation of the tested specimens, extended time studies for the coal imbibition were carried out. The mass gain of the tested specimens versus immersing time is plotted in Fig. 3. The results revealed no further significant changes to the sample mass after 80 h which indicated full saturation of the specimen. The weight percent of imbibed water for the 45 saturated samples varies from 1.2 to 2.4 %.

2.2 Experimental Setup and Procedure

A SHPB system was employed to conduct dynamic BD tests on both dry and saturated coals. The testing system consists of identical incident and transmitter bars with 50 mm in diameter and 2.0 m in length. The device incorporates a gas gun to accelerate the cylindrical steel striker bar (50 mm in diameter and 400 mm in length). Semi-conductor strain gauges were affixed on the incident and transmitter bars to record the elastic waves. The SHPB

testing system is illustrated in Fig. 4. Prior to each test, the coal specimen was sandwiched between the incident and transmitter bars. Then, an impact shock on the incident bar was generated by the high-speed striker bar ejected by the gas gun. Due to this impact shock pulse, an input strain wave $\varepsilon_I(t)$ was generated in the incident bar. When the input strain wave reached the interface between the specimen and incident bar, a portion of the strain wave was reflected back to the incident bar, which was recorded as reflected strain wave $\varepsilon_R(t)$, and the remaining portion was transmitted through the specimen to the transmitter bar recorded as transmission strain wave $\varepsilon_T(t)$. Using these three recorded strain waves, the normal loading force $P(t)$ and displacement $U(t)$ can be calculated using the following equations:

$$P(t) = EA \frac{(\varepsilon_I(t) + \varepsilon_R(t) + \varepsilon_T(t))}{2} \tag{1}$$

$$U(t) = C \int_0^t (\varepsilon_I(t) - \varepsilon_R(t) - \varepsilon_T(t)) \tag{2}$$

where E is the Young's modulus and A is cross-sectional area of the bar. E is equal to 200 GPa for the two bars in

Table 2 Final results of the dynamic indirect tensile test on 24 water-saturated coal specimens

Specimen ID	Bedding direction (°)	Impact velocity (m/s)	Strain rate (s^{-1})	Failure time (μs)	Dynamic indirect tensile strength (MPa)
321	0.0	2.112	37.995	191	3.753
331	0.0	1.58	24.743	203	2.940
3101	0.0	3.221	67.791	142	5.087
3102	0.0	2.754	58.352	163	4.480
3121	0.0	2.851	55.977	160	4.137
513	0.0	2.147	37.029	189	3.809
131	22.5	2.529	50.175	173	4.698
171	22.5	3.233	60.951	140	5.088
172	22.5	3.196	62.581	145	4.897
3122	22.5	2.573	50.652	170	4.478
521	22.5	2.476	41.347	181	4.191
341	45.0	3.132	63.931	151	5.226
351	45.0	3.308	62.773	140	5.330
352	45.0	3.784	71.976	123	5.757
241	45.0	2.915	58.021	156	4.95
242	45.0	3.02	53.984	152	5.051
371	67.5	3.363	58.163	137	5.506
381	67.5	3.435	61.589	133	5.528
442	67.5	2.878	54.995	161	4.756
372	90.0	3.041	54.015	147	5.134
391	90.0	3.15	55.894	149	5.306
461	90.0	3.09	56.419	146	5.252
672	90.0	2.347	34.137	190	4.439
623	90.0	2.084	35.632	198	3.981

Fig. 5 Dynamic force balance check for two typical dynamic BD tests. **a** Air dry specimen No. 211 with the impact velocity of 3.213 m/s and the bedding angle of 0°. **b** Water-saturated specimen No. 351 with the impact velocity of 3.308 m/s and the bedding angle of 45° (color figure online)
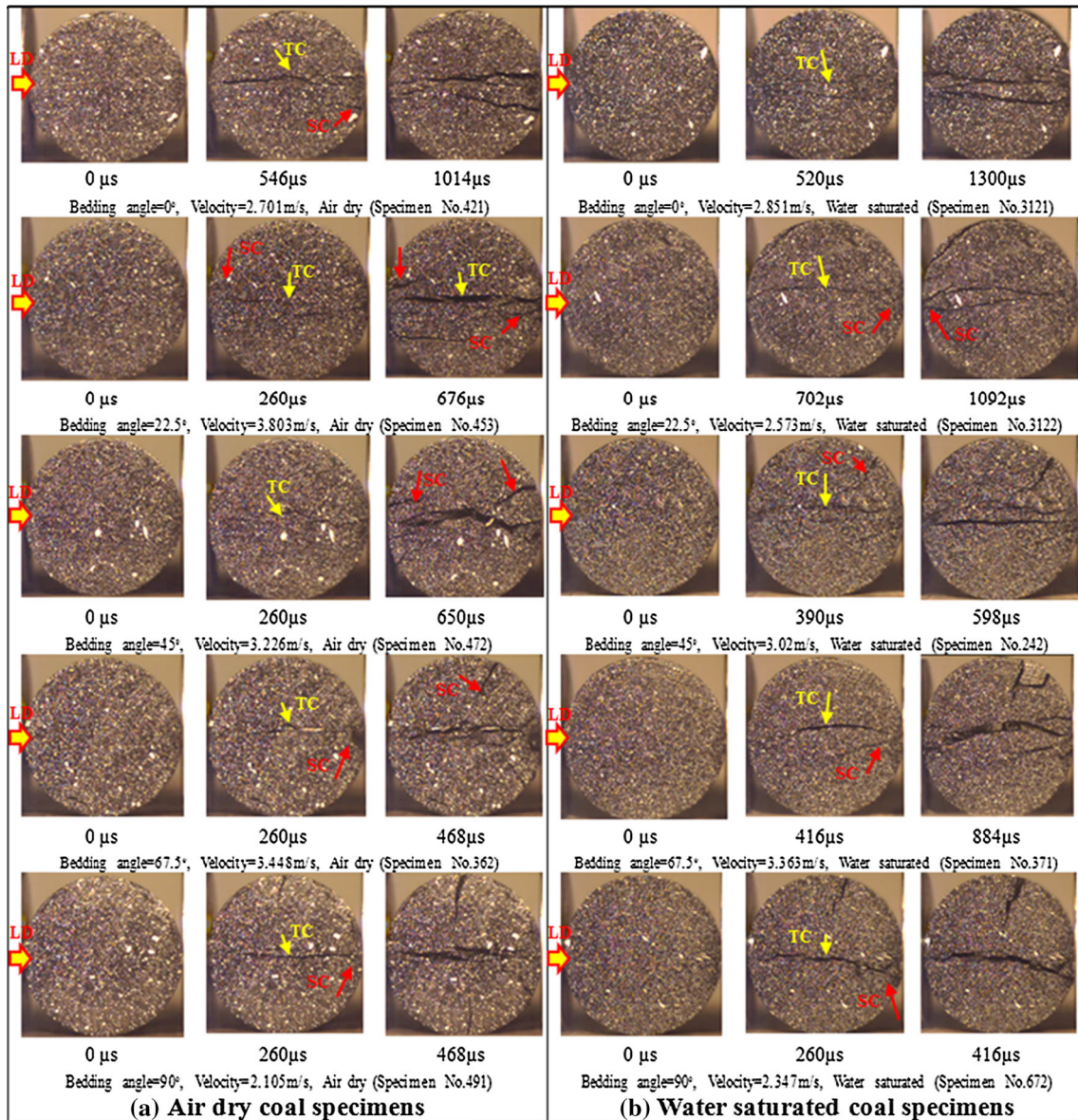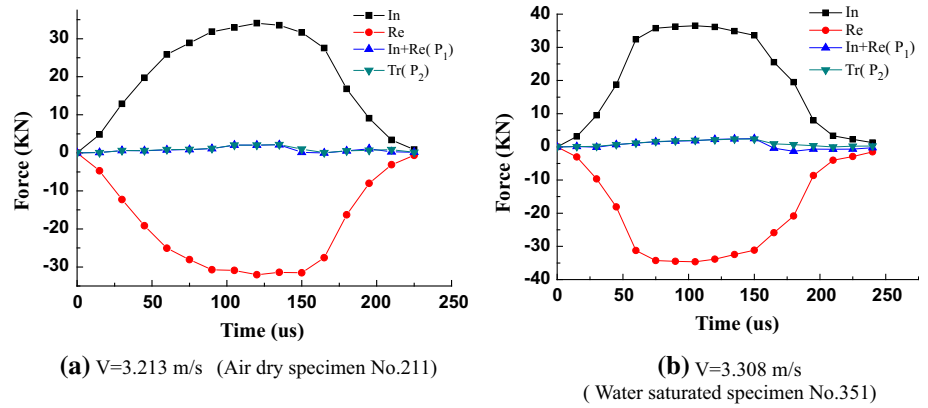

(a) V=3.213 m/s   (Air dry specimen No.211)

(b) V=3.308 m/s
(Water saturated specimen No.351)

Fig. 6 Failure photos with different bedding angles. *Red arrow* the shear cracks (SC). *Yellow arrow* the main tensile cracks (TC). *LD* loading direction (color figure online)

(a) Homogeneous and isotropic rock

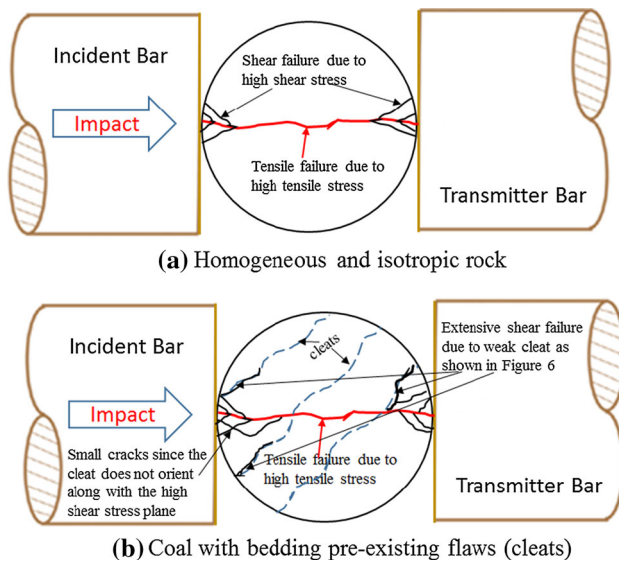**(b)** Coal with bedding pre-existing flaws (cleats)

Fig. 7 Conceptual illustration of the rock with and without preexisting flaws in SHPB tests

the current experimental system. C is the one-dimensional longitudinal stress wave velocity of the incident/transmitter bar. The indirect tensile strength of the coal specimen was then calculated using the following equation (Bieniawski and Hawkes 1978);

$$\sigma_t = \frac{2P_{max}}{\pi DL} \tag{3}$$

where L is the thickness of the specimen (25 mm), D is the diameter of the specimen (50 mm), and P_{max} is the maximum value of the loading force, $P(t)$.

The strain rate ($\dot{\varepsilon}(t)$) of the coal specimen, which reflects the loading condition of the SHPB test is

$$\dot{\varepsilon}(t) = C(\varepsilon_I(t) - \varepsilon_R(t) - \varepsilon_T(t)) \tag{4}$$

Another common index used to reflect the dynamic loading condition is the loading rate ($\dot{\sigma}_t$), which can be obtained as

$$\dot{\sigma}_t = \frac{\sigma_t}{t_d} \tag{5}$$

where t_d is the time when $P(t)$ reaches its peak value. More details on the dynamic indirect tensile test using a SHPB can be found in the work of Dai et al. (2010).

During the test, the strain gauge signals are recorded using a HS-digital oscilloscope with a sampling rate and a 12-bit isolation module. All of the raw data generated by the strain gauge are processed and digitally filtered with a low-pass filter with a cutoff frequency of 10,000 Hz. This is used to remove the very high frequency noise (Zhang and Zhao 2013b). To qualitatively characterize the failure pattern of the post-failure specimens, a high-speed camera (Photron FASTCAM SA1.1 model 675K-CI) was used in

the study. The detailed information on the components of the HS-camera can be found in the work of Zhang and Zhao (2013b). In the present study, the image resolution of the HS-camera was set to be 384×352 pixels and the frame frequency was 37,500 fps (26 μs between two adjacent images). It was post triggered at the time of major specimen fragmentation and located at a safe distance of 0.5 m from the specimen to avoid damage and camera motion induced by the ejecting fragments. For each specimen, the majority of broken fragments and particles were collected and analyzed for the size distribution for both dry and saturated specimens.

3 Results and Discussion

Only 32 dry specimens and 24 saturated specimens were successfully tested for dynamic BD tensile strength. The experimental results including the impact velocity, the strain rate, the loading rate and the dynamic indirect tensile strength for both dry and saturated specimens are listed in Tables 1 and 2. According to the ISRM suggested method (Zhou et al. 2012), dynamic force balance on all SHPB tests has to be checked. To ensure the validity of Eqs. 3 and 5, the force balance was checked, and the results are shown in Fig. 5. Theoretically, the dynamic force on one side of the tested specimen is proportional to the summation of the incident (In, labeled as black squares in Fig. 5) and reflected (Re, labeled as red solid dots in Fig. 5) stress waves. The total summation of these two is shown as blue triangles in the figure. On the other side of the specimen, the dynamic force is proportional to the transmitter bar (Tr, labeled as green triangle in Fig. 5) stress wave. It is notable that the dynamic forces on both sides of the specimen are almost identical during the whole dynamic loading period. Thus, there is no global force difference in the specimen to induce the inertial effects (Chen et al. 2009; Dai 2010). Therefore, we can use the static tensile strength formula (Eq. 3) to analyze the obtained dynamic results.

3.1 Fracture Morphology and Failure Mode

Figure 6 shows the dynamic evolution of the fracture initiation and propagation towards failure for both dry (Fig. 6a) and saturated (Fig. 6b) specimens using the high-speed camera. It can be found that the bedding angle influences the final fracture patterns for both dry and saturated coals in the dynamic BD tensile tests. When the impact shock load was either parallel ($\theta = 0°$) or perpendicular ($\theta = 90°$) to the bedding plane, the tensile failure along the impact direction was the dominant failure mode illustrated in the first and last rows in Fig. 6. When the bedding plane was neither parallel nor perpendicular to the

Fig. 8 Relationship of stress and displacement of water-saturated coals and air dry coals with various bedding angles under selected loading speed. From **a–e**, the bedding angle is 0°, 22.5°, 45°, 67.5° and 90°, respectively

(a) Bedding angle=0°

(b) Bedding angle=22.5°

(c) Bedding angle=45°

(d) Bedding angle=67.5°
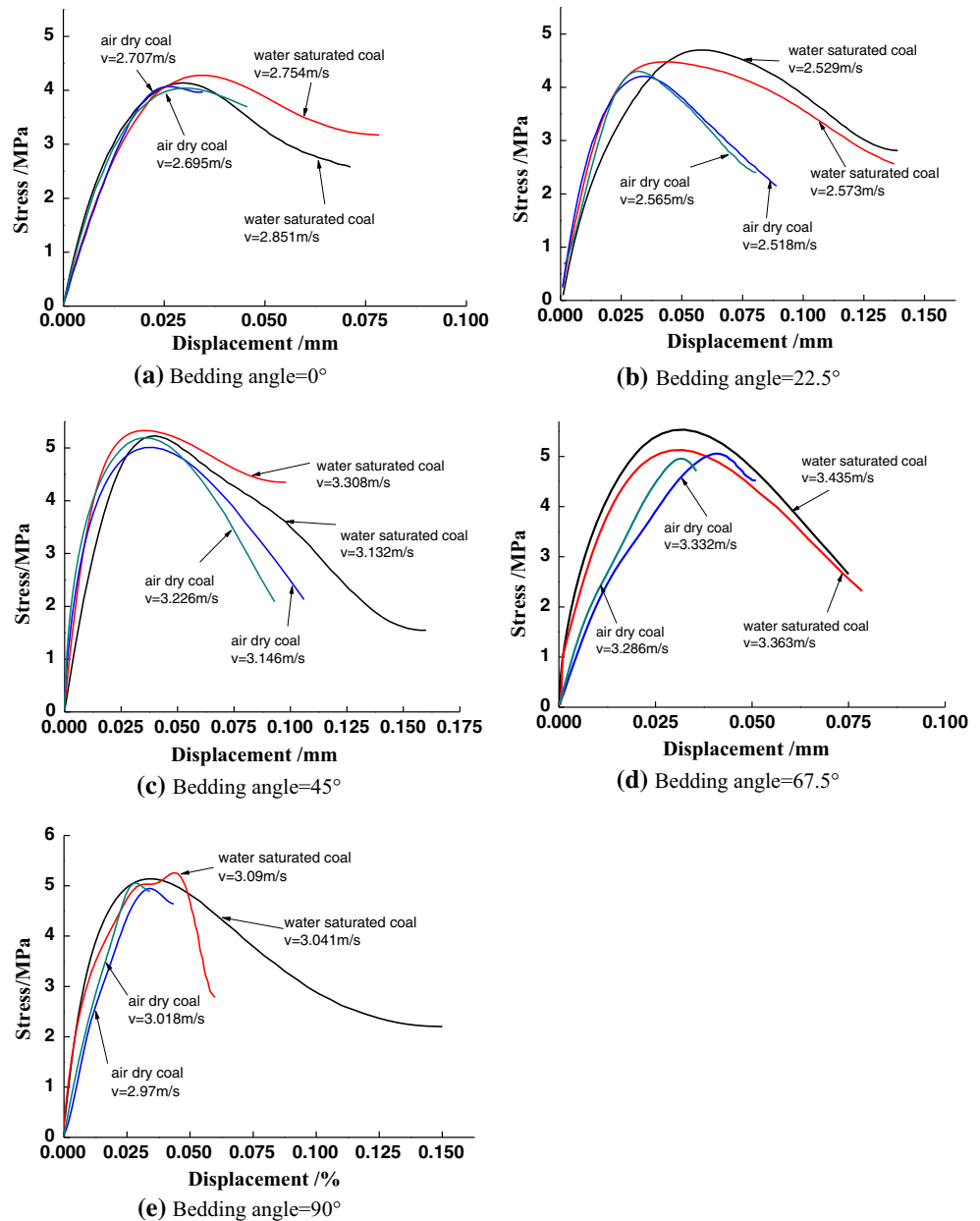
(e) Bedding angle=90°

impact direction, although the tensile failure was still the dominant failure model, shear failure zones at the two contact ends were observed as shown in the 2nd, 3rd and 4th rows in Fig. 6 with bedding angles of 22.5°, 45° and 67.5°, respectively. These shear zones may be attributed to the localized high shear stress concentration along the weak fracture/bedding planes resulting from the high loading/strain rate.

In SHPB tests, the failure pattern of BD specimens usually includes both shear and tensile failures (Xia and Yao 2015; Zhang and Zhao 2013a, b, c; Zhou et al. 2012). When the BD specimen is homogeneous and isotropic, the tensile failure initiates in the center of the disc and the crack is parallel to the impact direction as shown in Fig. 7a.

The tensile crack quickly propagates and divides the BD specimen into two pieces. As soon as the tensile crack divides the specimen, the state of stress at both contact ends will be redistributed because the specimen is no longer intact. Each half of the disc will behave like semi-circular rock disc. Two shear zones developed at both contact ends for each semicircular rock disc since the localized high shear stress concentrations accumulated with time. Because the rock is homogeneous and isotropic, the shear failure zones are symmetric as illustrated in Fig. 7a. However, for the rock with pre-existing flaws, the failure pattern of the BD specimen was expected to be much more complex. As shown in Fig. 7b, the tensile failure is still the dominant failure mode because of the
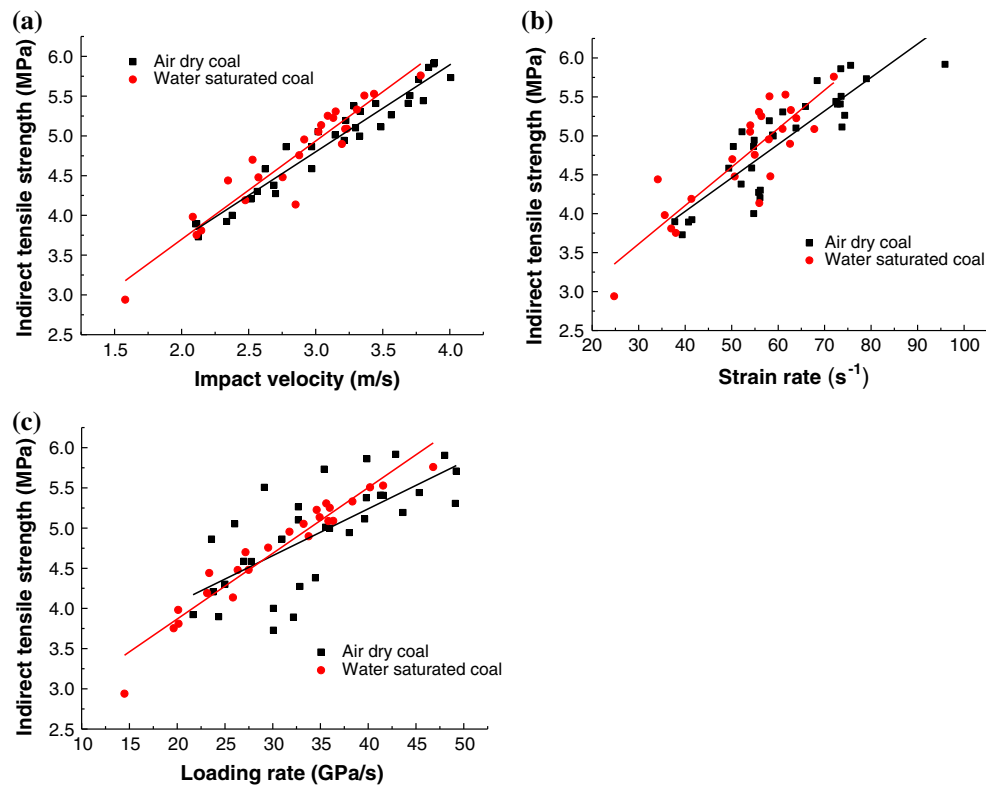
Fig. 9 The relationships between the impact velocity, the strain rate and the loading rate and the dynamic indirect tensile strength: **a** the dynamic tensile strength versus the impact velocity; **b** the dynamic tensile strength versus the strain rate; **c** the dynamic tensile strength versus the loading rate

high tensile stress and low tensile strength of the rock. But the shear failure zone is much more complex because of the weak planes, cracks/cleats in the coal. If the crack plane aligns with the high shear stress plane, extensive shear cracks will develop along the weak cleats and the shear failure zone is not symmetric as shown in Fig. 7b. Our experimental results show the similar failure pattern. In Fig. 6, when the bedding angles are 22.5° and 45°, extensive shear failure was observed at the end of the failure process.

Based on the results and analysis, we can conclude that the failure pattern of BD specimens for cracked rock, such as coal, is complex, especially for the shear failure zones at the contact ends. The shear failure pattern is not only loading rate dependent as discussed in previous studies (Xia and Yao 2015; Zhang and Zhao 2013a, b, c), but also the bedding angle dependent as shown in Figs. 6 and 7.

3.2 Tensile Strength Results

During the test, the load–displacement curves were continuously monitored and recorded, and were subsequently used to estimate the corresponding indirect tensile strength using Eq. (3). Figure 8 shows the typical results of load–displacement curves for dry and saturated specimens under impact loading. It can be seen that the load–displacement curves for each saturated specimen showed a smooth post-failure tail with extensive deformation. Comparatively speaking, the load–displacement curves of dry specimens are characterized by a smaller peak strength and deformation before their final failure. The measured indirect tensile strengths for both dry and saturated specimens with various bedding angles are shown in Fig. 9. The indirect tensile strengths are plotted versus impact velocity, strain rate and loading rate as shown in Figs. 9a–c. The regressed linear trends for both dry and saturated coals are also plotted in Fig. 9. As expected, it was found that the indirect tensile strengths for both dry and saturated coals are rate dependent and increased with higher impact velocity, strain rate and loading rate. Moreover, the loading rate dependency of the tensile strengths for saturated specimens was found to be stronger than for dry specimens as presented in Fig. 9c. The same phenomenon was also observed for sandstones by Ogata et al. (2004) and Huang et al. (2010).

From Fig. 9, no decrease of dynamic tensile strengths for saturated coals, compared with dry specimens, was observed as other researchers reported for other rocks (Huang et al. 2010). Interestingly, we found the tensile strength of saturated specimens is larger than the dry one at high impact velocity. This phenomenon is thought to be
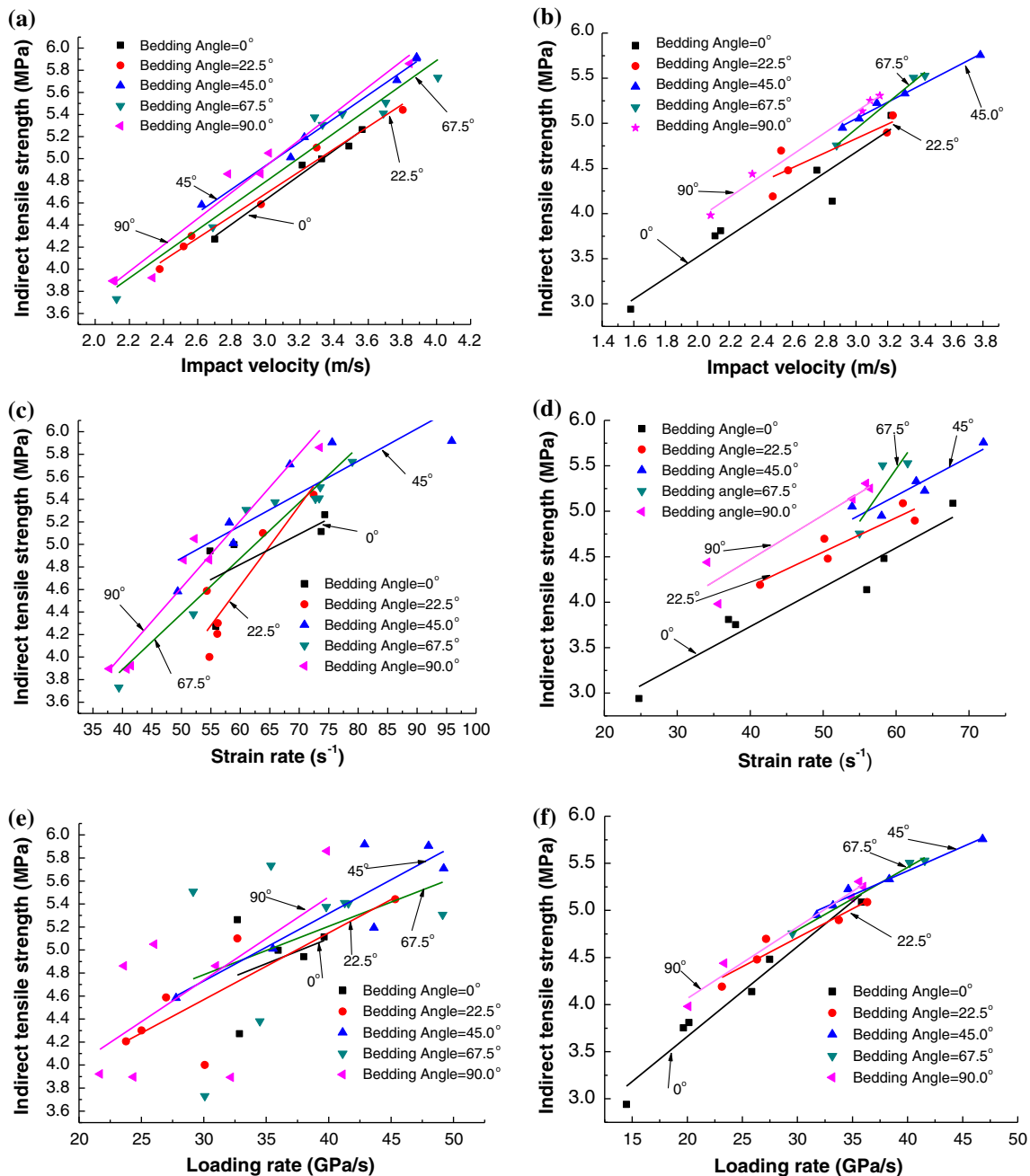
Fig. 10 Dynamic indirect tensile strength versus impact velocity, strain rate and loading rate for air dry and water-saturated coal specimens with different bedding directions from the SHPB test. **a**, **c** and **e** for the air dry specimens. **b**, **d** and **f** for the water-saturated specimen

attributable to the Stefan effect (Rossi 1991). For saturated coals, the presence of free water in the micro-pores or micro-cracks can form thin viscous water films between the adjacent walls of pores or cracks and these thin films tend to induce an opposing force when an attempt is made to break the microstructure (micro-cracking) at high strain/ loading rate. This will translate to an increase of the dynamic tensile strength at high strain/loading rate for saturated coals compared to dry ones as shown in Fig. 9.

Figure 10 shows the variations of dynamic tensile strengths with different bedding angles under various impact velocities, strain rates and loading rates for both dry and saturated coals. For dry coals, Fig. 10a shows that the effect of impact velocity on the dynamic indirect tensile strength was similar for all the bedding angles, as the slope of the fitting linear is almost the same. Moreover, Fig. 10a also indicates that the bedding angles have less effect on the dynamic tensile strength compared to the impact

velocity. Unlike the impact velocity, the experimental results were much more dispersed for strain rate (Fig. 10c) and loading rate (Fig. 10e). For saturated coals, it can be found that the coal specimens with the 0° bedding angle are easiest to be broken under the indirect dynamic tensile loading as shown in Fig. 10b at which the 0° bedding angle strength line is lowest. Figure 10f shows the stronger loading rate dependence of dynamic indirect tensile strength for water-saturated specimens than for dry ones since the dry specimens shown in Fig. 10e are more scattered compared to the saturated ones. The loading rate dependency of tensile strength is believed to be attributed to the viscous cohesive stress of free water in the coal.

4 Conclusions

The objective of this work was to investigate the dynamic indirect tensile failure features of dry and saturated coals comparatively. 32 dry specimens and 24 water-saturated specimens were successfully used to measure the dynamic indirect tensile strength in the SHPB tests. The following main conclusions can be drawn:

- The saturated specimens have relatively stronger loading rate dependence than the dry coals.
- Both shear and tensile failures were observed for tested coal specimens.
- The bedding angle has a smaller effect on the dynamic indirect tensile strength of coal compared to the impact velocity.
- Saturated coal specimens have higher indirect tensile strength than dry ones.

References

Asprone D, Cadoni E, Prota A, Manfredi G (2009) Dynamic behavior of a Mediterranean natural stone under tensile loading. Int J Rock Mech Min Sci 46:514–520

ASTM D5142–09 (2009) Standard test methods for proximate analysis of the analysis sample of coal and coke by instrumental procedures. ASTM International, West Conshohocken

Bieniawski ZT, Hawkes I (1978) Suggested methods for determining tensile strength of rock materials. Int J Rock Mech Min Sci Geomech Abstr 15:99–103

Broch E (1979) Changes in rock strength by water. In: Proceedings IV international society of rock mechanics. Montreux, pp 71–75

Burshtein LS (1969) Effect of moisture on the strength and deformability of sandstone. J Min Sci 5:573–576

Cai M, Kaiser PK, Suorineni F, Su K (2007) A study on the dynamic behavior of the Meuse/Haute-Marne argillite. Phys Chem Earth Parts A/B/C 32:907–916. doi:10.1016/j.pce.2006.03.007

Chen R, Xia K, Dai F, Lu F, Luo SN (2009) Determination of dynamic fracture parameters using a semi-circular bend technique in split Hopkinson pressure bar testing. Eng Fract Mech 76:1268–1276. doi:10.1016/j.engfracmech.2009.02.001

Cho SH, Ogata Y, Kaneko K (2003) Strain-rate dependency of the dynamic tensile strength of rock. Int J Rock Mech Min Sci 40:763–777

Colback PSB, Wiid BL (1965) The influence of moisture content on the compressive strength of rock. In: Proceedings of the third Canadian rock mechanics symposium, pp 65–83

Dai F (2010) Dynamic tensile, flexural and fracture tests of anisotropic barre granite. Dissertation, University of Toronto

Dai F, Xia K, Tang L (2010) Rate dependence of the flexural tensile strength of Laurentian granite. Int J Rock Mech Min Sci 47:469–475

Dutta PK, Kim K (1993) High-strain-rate tensile behavior of sedimentary and igneous rocks at low temperatures. U.S. Army Cold Regions Research and Engineering Laboratory, Hanover, NH

Fuenkajorn K, Kenkhunthod N (2010) Influence of loading rate on deformability and compressive strength of three Thai sandstones. Geotech Geol Eng 28:707–715

Goldsmith W, Sackman JL, Ewerts C (1976) Static and dynamic fracture strength of Barre granite. Int J Rock Mech Min Sci Geomech Abstr 13:303–309

Gong F-Q, Zhao G-F (2013) Dynamic indirect tensile strength of sandstone under different loading rates. Rock Mech Rock Eng. doi:10.1007/s00603-013-0503-7

Han G (2003) Rock stability under different fluid flow conditions. Dissertation, University of Waterloo

Hawkins AB, Mcconnell BJ (1992) Sensitivity of sandstone strength and deformability to changes in moisture-content. Q J Eng Geol 25:115–130

Howe S, Goldsmith W, Sackman J (1974) Macroscopic static and dynamic mechanical properties of Yule marble. Exp Mech 14:337–346

Huang S, Xia K, Yan F, Feng X (2010) An experimental study of the rate dependence of tensile strength softening of Longyou sandstone. Rock Mech Rock Eng 43:677–683. doi:10.1007/s00603-010-0083-8

ISRM, International Society for Rock Mechanics (1978) Commission on Standardization of Laboratory and Field Tests. Suggested methods for determining tensile strength of rock materials. Int J Rock Mech Min Sci Geomech Abstr 15:99–103

Khan AS, Irani FK (1987) An experimental study of stress wave transmission at a metallic-rock interface and dynamic tensile failure of sandstone, limestone, and granite. Mech Mater 6:285–292

Li Z, Reddish D (2004) The effect of groundwater recharge on broken rocks. Int J Rock Mech Min Sci 41:280–285

Mclamore R, Gray KE (1967) Mechanical behavior of anisotropic sedimentary rocks. J. Eng. Ind. 89:62–67

Ogata Y, Jung W, Kubota S, Wada Y (2004) Effect of the strain rate and water saturation for the dynamic tensile strength of rocks. Explos Shock Wave Hyperveloc Phenom Mater 465–466:361–366

Ray SK, Sarkar K, Singh TN (1999) Effect of cyclic loading and strain rate on the mechanical behaviour of sandstone. Int J Rock Mech Min Sci 36:543–549

Rossi P (1991) A physical phenomenon which can explain the mechanical behaviour of concrete under high strain rates. Mater Struct 24:422–424

Scholtès L, Donze F-V, Khanal M (2011) Scale effects on strength of geomaterials, case study: coal. J Mech Phys Solids 59:1131–1146

Wang QZ, Li W, Xie HP (2009) Dynamic split tensile test of flattened Brazilian disc of rock with SHPB setup. Mech Mater 41:252–260

Xia K, Yao W (2015) Dynamic rock tests using split Hopkinson (Kolsky) bar system-A review. J Rock Mech Geotech Eng 7:27–59

Xia K, Huang S, Jha AK (2010) Dynamic tensile test of coal, shale and sandstone using split Hopkinson pressure bar: a tool for blast and impact assessment. Int J Geotech Earthq Eng 1:24–37. doi:10.4018/jgee.2010070103

Yan F, Feng XT, Chen R, Xia K, Jin C (2012) Dynamic tensile failure of the rock interface between tuff and basalt. Rock Mech Rock Eng 45:341–348

Zhang QB, Zhao J (2013a) A review of dynamic experimental techniques and mechanical behaviour of rock materials. Rock Mech Rock Eng. doi:10.1007/s00603-013-0463-y

Zhang QB, Zhao J (2013b) Effect of loading rate on fracture toughness and failure micromechanisms in marble. Eng Fract Mech 102:288–309

Zhang QB, Zhao J (2013c) Determination of mechanical properties and full-field strain measurements of rock material under dynamic loads. Int J Rock Mech Min Sci 60:423–439. doi:10.1016/j.ijrmms.2013.01.005

Zhao J, Li HB, Wu MB, Li TJ (1999) Dynamic uniaxial compression tests on a granite. Int J Rock Mech Min Sci 36:273–277

Zhou YX, Xia K, Li XB, Li HB, Ma GW, Zhao J, Zhou ZL, Dai F (2012) Suggested methods for determining the dynamic strength parameters and mode-I fracture toughness of rock materials. Int J Rock Mech Min Sci 49:105–112. doi:10.1016/j.ijrmms.2011.10.004